Title
Pure and Zn-doped Pt clusters go flat and upright on MgO(100)

Journal
Physical Chemistry Chemical Physics, 16(48)

ISSN
0956-5000

Authors
Shen, Lu
Dadras, Jonny
Alexandrova, Anastassia N

Publication Date
2014-12-28

DOI
10.1039/c4cp01877j

Peer reviewed

Volume 16 | Number 48 | 28 December 2014 | Pages 26393–27136

PCCP

Physical Chemistry Chemical Physics

www.rsc.org/pccp

Includes a collection of articles on Size Selected Clusters and Particles

ISSN 1463-9076

ROYAL SOCIETY OF CHEMISTRY

PAPER

Anastassia N. Alexandrova *et al.*

Pure and Zn-doped Pt clusters go flat and upright on MgO(100)

PCCP

PAPER

View Article Online
View Journal | View Issue

Pure and Zn-doped Pt clusters go flat and upright on MgO(100)†

Cite this: *Phys. Chem. Chem. Phys.*, 2014, **16**, 26436

Lu Shen,‡[a] Jonny Dadras‡[a] and Anastassia N. Alexandrova*[ab]

Pure and doped sub-nanoclusters can exhibit superb catalytic activity, which, however, strongly depends on their size, shape, composition, and the nature of the support. This work is about surface-deposited sub-nano Pt-based clusters, which are promising catalysts for the reactions of dehydrogenation. Using density functional theory and *ab initio* calculations, and an *ab initio* genetic algorithm for finding the global minima of clusters, we found a peculiar effect that Pt_5 and Pt_4Zn clusters exhibit upon deposition on MgO(100). Both of them change shapes from the gas phase 3-D form to a planar form, and they stand upright on the support. Several reasons are responsible for this behaviour. In part, clusters go flat due to the electron transfer from the support. Indeed, the anionic Pt_5^- and Pt_4Zn^- species are flat also in the gas phase. Charging induces the second-order Jahn–Teller effect (or partial covalency) facilitated by the recruitment of the higher-energy 6p atomic orbitals on Pt into the valence manifold, and that is the reason for the planarization of the anions. Secondly, clusters maximize interactions with the surface O atoms (resulting in further favouring of 2-D structures over 3-D), and avoid contacts with surface Mg atoms (resulting in upright morphologies).

Received 30th April 2014,
Accepted 22nd May 2014

DOI: 10.1039/c4cp01877j

www.rsc.org/pccp

Introduction

Small surface-deposited clusters offer exciting applications for catalysis. The catalytic properties of such nanometer and sub-nanometer clusters can be outstanding, but depend strongly and nonlinearly on cluster size and composition,[1–7] and also on the nature of the support.[6,8–13] The electronic structure of clusters is reminiscent of molecules, in that important chemical–physical properties can be understood from a molecular orbital (MO) picture, wherein the MOs will be well-separated in energy, rather than having continuous energy bands.[14,15] The support plays the role of a ligand in very small (<1 nm) clusters, capable of actively modifying cluster structures, charge, and other properties (see *e.g.* in ref. 7). In this field, *ab initio* theory has been utilized recently on the charge transfer from TiO_2(110) surface to the mounted Au_{20} clusters.[16] Others also have uncovered the partial charge transfer from a defected MgO(100) surface to the clusters bound to the oxygen-vacancy.[17] Such an effect acts as an essential feature for the promotion of the chemical activity of clusters. Given that the selectivity and activity of the cluster will depend upon the number of vertex and edge atoms present, quantifying support-dependent effects to the cluster morphology becomes a matter of central importance. The present work is one that addresses the fundamental understanding of the effect of the support on cluster morphology, through the insight of electronic structure.

We focus on small surface-mounted Pt-based clusters. These systems are of potential interest to reactions of catalytic dehydrogenation of alkanes, producing alkenes and hydrogen gas.[18–26] Not long ago, it was found that zeolites impregnated with Pt and Zn may present an inexpensive alternative to Pt–Sn–zeolites—Zn being about 10% the cost of Sn—for the dehydrogenation of alkanes; specifically for dehydrogenation of isobutane to isobutene and propane to propene.[27] Also, it was found by Galvita *et al.*[19] that the addition of Sn to Pt on hydrotalcite (PtSn/Mg(Al)O) promoted the activity of dehydrogenation of ethane to ethene, while simultaneously reducing coke build up when compared with Pt/Mg(Al)O. The MgO(100) surface in general is highly studied as a supporting material for metal clusters.[28,29] Hence, motivation exists to investigate a model system of sub-nanometer Pt and Pt–Zn clusters deposited on MgO(100) surfaces. It is noted that, previously, others have shown that nanometer sized clusters of group 10 elements (in particular, clusters of Pt, Pd, and Pt-based bi-metallics) undergo morphological changes when deposited on oxide supports, including MgO.[30–32] In this report, the specific case of surface mounted Pt_5 and Pt_4Zn

[a] *Department of Chemistry and Biochemistry, University of California, Los Angeles, California, 90095-1569, USA. E-mail: ana@chem.ucla.edu*
[b] *California NanoSystems Institute, 570 Westwood Plaza, Building 114, Los Angeles, CA 90095, USA*

† Electronic supplementary information (ESI) available: Calculated relative energies for the 2-D and 3-D isomers calculated at various levels of *ab initio* theory, pictures of valence MOs of the considered cluster anions in the gas phase and clusters on the support, and the picture of the valence MO of the Li_5^- cluster. See DOI: 10.1039/c4cp01877j

‡ These authors equally contributed to this work.

clusters on MgO is shown to exhibit dramatic changes in morphology, relative to gas-phase structures, after surface deposition. This effect is explained *via ab initio* calculations and chemical bonding analysis.

Methods

The calculations for surface-supported clusters were performed at the DFT level with a plane wave (PW) basis set and ultra-soft pseudo-potentials implemented in *Quantum Espresso*.[33–36] The cutoff energy for the plane wave basis set and the density was chosen to be 435 eV and 4350 eV, respectively; the Perdew–Burke–Ernzerhof (PBE) functional was employed.[37] All PW-DFT calculations were spin-polarized; spin-unrestricted calculations with fixed multiplicity were performed for gas-phase clusters. The MgO(100) surface was modelled by a slab with $3 \times 3 \times 3$ unit cells per supercell and a $1 \times 1 \times 1$ Monkhorst–Pack grid with shifts in k_x and k_y. The vacuum separation between the top of the surface and the bottom of its image along z was 12.44 Å. Only the stoichiometric surface was considered in this study, because it is known that clusters of Pt and Pd whose d-AOs are so full avoid O vacancies, unlike clusters on Au that have a high affinity to them, because of the relativistic stabilization of the 6s-AOs in Au. The atomic charges were assigned through the Bader analysis.[38–40] For clusters in the gas phase, we used the UTPPSh,[41] CASSCF,[42–47] and MP2[48–53] levels of theory with the aug-cc-pVTZ+ECP basis set[54] implemented in Gaussian 09.[55] We used these calculations to confirm the adequate performance of PW-DFT for the studied systems. The results were found to agree across theoretical methods, as shown in the ESI.† All data presented in the main text were obtained using PW-DFT, for consistency. The MOs were plotted at the Γ point, using the periodic implementation of DFT in *Quantum Espresso*. The search for the global minimum structures in the gas phase was done using our Gradient Embedded Genetic Algorithm (GEGA)[56,57] at UPBE/LANL2DZ. The searches on the supporting surface were done by hand, using the gas phase local minima as guidance. The GEGA produced a highly diverse population of 2-D and 3-D minima, which were then placed on the support in different ways, as starting points in the search. We realize the inherent deficiency in this process, and adopt it only as a compromise in view of exceptional cost of the stochastic search for supported clusters.

Results and discussion

Cluster structures

Fig. 1 shows the lowest energy minima of the gas phase and surface deposited Pt_5 and Pt_4Zn clusters. The relative energies of the gaseous clusters were confirmed at various levels of theory discussed in the Methods section (see ESI,† Table S1). There is a remarkable change in structure as the clusters undergo surface deposition. Both Pt_5 and Pt_4Zn have a 3-D trigonal-bipyramidal shape in the gas phase. This is a clear indication of delocalized bonding governing the globular shapes of these clusters, as is the case in many metallic clusters. There are also 2-D isomers, found to be at least 0.31 eV higher in energy for Pt_5 and 0.11 eV for Pt_4Zn. However, on MgO(100) both clusters become planar. Most unusually, they do not lie down and wet the support; instead, they stand upright in a planar trapezoidal form. This remarkable structural effect attracted our attention, and resulted in this communication. The deposited clusters also have isomers that have 3-D shapes (Fig. 1), but those are found to be significantly less stable. In Table 1 we report relative energies, atomization energies, and cluster–surface binding energies for the clusters of interest.

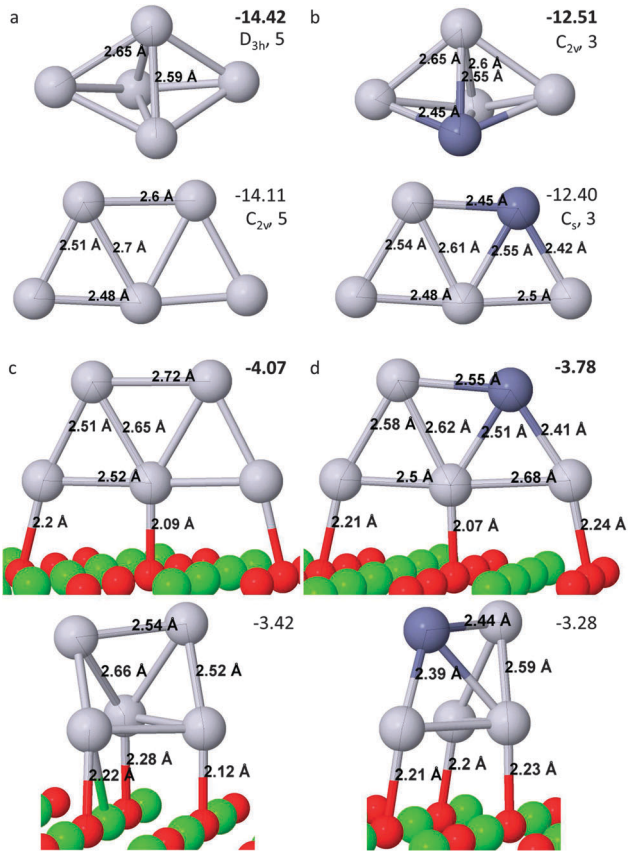

Fig. 1 Global and low energy local minima for the studied clusters: (a) Pt_5 in the gas phase; (b) Pt_4Zn in the gas phase; (c) Pt_5 on MgO(100); and (d) Pt_4Zn on MgO(100). Pt is light gray, Zn is dark purple, O is red, and Mg is green. All energies are in eV, for (a) and (b), they are the formation energies of the clusters, the symmetry groups and the spin multiplicities are listed as well; (c) and (d) are the absorption energies of the clusters on the MgO(100) surface.

Why flat and upright?

We aimed at gaining understanding as to why the clusters undergo planarization upon deposition, from the point of view of their electronic structures. First, as depicted in Fig. 2, it is

Table 1 Formation/atomization energies of gas-phase clusters and binding energies of clusters to the support

	Pt_5, 3-D	Pt_5, 2-D	Pt_4Zn, 3-D	Pt_4Zn, 2-D
E_{form} (eV) gas phase	−14.42	−14.11	−12.51	−12.40
E_B (eV) to surface	−3.42	−4.07	−3.28	−3.78

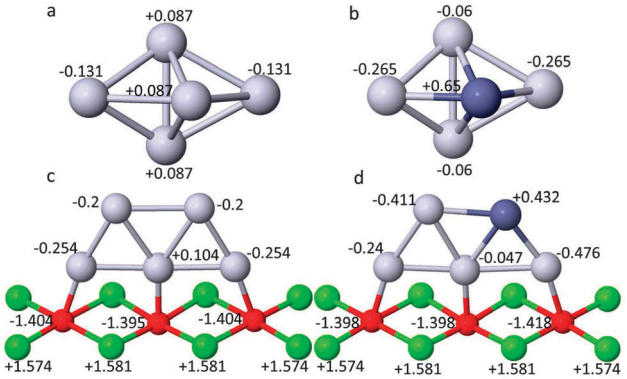

Fig. 2 Bader charges on atoms in gaseous and surface-deposited clusters: (a) Pt_5 in the gas phase, (b) Pt_4Zn in the gas phase, (c) Pt_5 on MgO(100), and (d) Pt_4Zn on MgO(100).

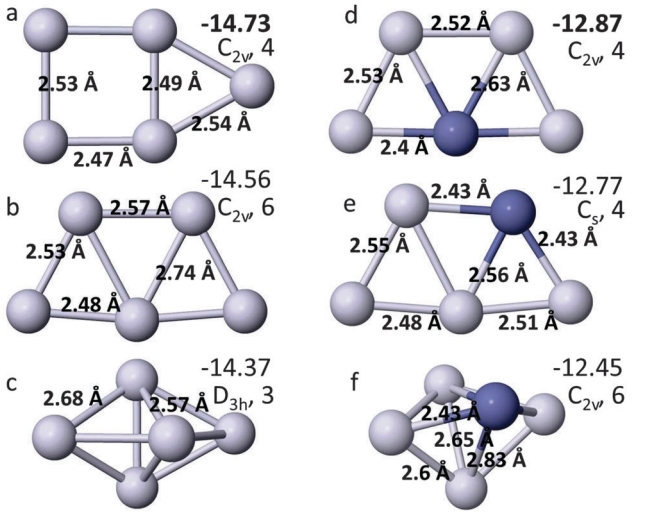

Fig. 3 The global and few lowest-energy isomers of Pt_5^- (a–c) and Pt_4Zn^- (d–f); listed formation energies are in eV, the symmetry groups and the spin multiplicities are listed as well.

noted that there is charge transfer to the clusters from the support, effectively making the surface-deposited clusters anionic. The total charge on deposited Pt_5 is −0.804, and that on Pt_4Zn is −0.742. The charge redistribution for the atoms of the surface is fairly localized to the area right beneath the bound clusters, the average charge of Mg and O over the entire support is 1.55 *e* and −1.55 *e*, respectively; while each O near the cluster is about 0.15 *e* less negative and each nearby Mg is about 0.03 *e* more positive. Thus, the systems exhibit local bonding effects, and electrons are drawn to the clusters mainly from surface O atoms. It is interesting that O vacancies are not required for charge transfer. The presence of Zn polarizes the clusters, *i.e.* Zn is strongly positively charged, in accord with relative electronegativities of Pt and Zn. Since changes in shape of clusters, upon charging, have been seen previously in other systems,[16,17] we suspected that this present change in morphology was due primarily to charging.

We performed a separate automated search for the global and local minima of the anionic Pt_5^- and Pt_4Zn^- clusters in the gas phase. It was found that, indeed, the Pt_5^- and Pt_4Zn^- anions are planar in their global minimum forms (Fig. 3). They also have 3-D isomers close in energy (Table S1, ESI†), but the point is that planar structures are majorly stabilized. In Fig. S2 and S3 (ESI†) we compare the valence MOs (Bloch states plotted at the Γ point) of the gas phase anions with −1 charge to those of the clusters on the MgO(100) support. One may see that these wave functions look nearly identical, only allowing for some mixing with the states of the surface O atoms in the MgO-supported case. Thus, the bonding within the anion is not too severely perturbed by the surface.

In what follows, we argue that planarization is due, in large, to the second-order Jahn–Teller effect, which also can be called partial covalency.[57–59] First, consider a much simpler system, the Li_5^- cluster, which has been extensively characterized theoretically and experimentally.[60,61] This cluster has three competing isomers: the flat trapezoidal isomer (just like Pt_5^- and Pt_4Zn^-), the trigonal bipyramidal isomer (similarly to the present 3-D clusters), and a square pyramidal isomer. The chemical bonding in the two systems is radically different (Fig. S4, ESI†). The light atom of Li mostly uses its 2s atomic orbitals (AOs) for bonding in clusters. The overlap of the spherically-symmetric 2s-AOs is maximized when the shape of the cluster is as compact and connected as possible, *i.e.* as in the 3-D isomer. With such a simple electronic constitution, the "globular" clusters of Li have been most successfully described using the superatom model.[62] Basically, this model views the MOs of a cluster being gigantic analogues of the hydrogen-like AOs populated in accord with the Aufbau principle and Hund's rule. However, the reason why the flat Li_5^- cluster is also so stable was puzzling. In it, the maximal globular overlap is jeopardized, so it should be highly unfavorable. The reason for this stabilization is in the second order Jahn–Teller effect. The "central" Li atom in the flat isomer (position analogous to Pt#3 in Fig. 4) undergoes a significant 2sp-hybridization of AOs, *i.e.* recruits the 2p-AO into the chemical bonding in this anion. The hybrids form more directional, covalent overlaps with the rest of the electron density in the cluster (Fig. S4, ESI†). Partial covalency is responsible for favouring the planar geometry. The partial covalent bonding effect has been attributed to several other planar metallic clusters, with more complicated electronic structures, $LiNa_5^-$,[63] $SiAl_4^-$, $GeAl_4^-$,[64] all of which, remarkably, are trapezoidal.

Returning to the Pt_5^- and Pt_4Zn^- clusters, and starting with Pt_5^-, Pt has a $[Xe]4f^{14}5d^{10}$ or $[Xe]4f^{14}5d^96s^1$ electronic configuration, and likes to be inert. In order to bind to other atoms in the cluster, it has to promote electrons from the 5d- to the 6s-set and also the 6p-set. The 6s and 6p-AOs then contribute to bonding MOs, and the hole(s) left behind in the 5d-set also increase the overall bonding character. This situation is analogous to that in Pd clusters.[6,13] With an additional electron being added to make an anion, there is a chance to further use more 6s- and also 6p-AOs on Pt in the valence set. Indeed, the Natural Bond Order[65] analysis performed at the UTPPSh/aug-cc-pVTZ level of theory shows for the trapezoidal clusters

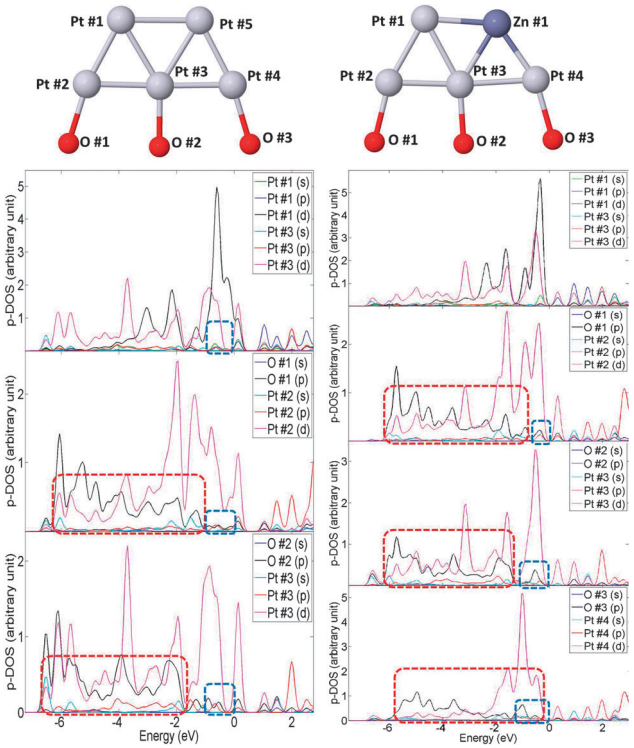

Fig. 4 p-DOS of the clusters on the MgO(100) surface: (left) Pt_5^- and (right) Pt_4Zn^-. Top to bottom: p-DOS for different atoms in the clusters are shown in each panel, to illustrate specifically the cluster–surface bonding and intra-cluster bonding. The Fermi energies are shifted to 0 eV. Outlined in red are covalent bonds between the Pt atoms and the O atoms in the MgO surface. Outlines in blue are the contributions of the 6p-states on Pt to the valence manifold.

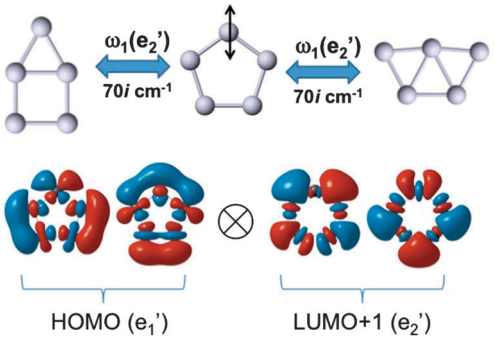

Fig. 5 Illustration of the second-order Jahn–Teller effect responsible for the formation of a partially covalent planar Pt_5^- structure. The α-HOMO − 1 and α-LUMO + 1 MOs mix through the normal mode corresponding to the imaginary frequency of the D_{5h} structure, leading to the C_{2v} structure.

that the 6s-AOs on Pt are populated by 0.8–1.1/0.9–1.0 electrons, and the 6p-AOs on Pt are populated by 0.1–0.4/0.1–0.2 electrons (in Pt_5^-/Pt_4Zn^-, respectively). The 6s- and 6p-AOs are close enough in energy to the 5d-AOs, and so they mix, making it impossible to uncover their isolated contributions to the MOs. We therefore operate rather blindly, and rely on the mixing observed in the p-DOS (contributions from the 6p-AOs are outlined in blue in Fig. 4).

To further demonstrate the presence of the second-order Jahn–Teller induced distortion, calculations on the gas phase anionic cluster of a perfect pentagon (found to be D_{5h}, $^4E_2'$) were performed. It is a saddle point, and the imaginary frequency of 70i cm^{-1} in it leads to the C_{2v} structures a and b in Fig. 3. We hypothesize that this normal mode vibronically couples the valence set with the higher-energy 6p-AOs for an increased covalent overlap. The symmetry of the vibration that causes the coupling must be contained in the reducible representation that is a direct product of the reducible representations corresponding to the two MOs in the D_{5h} system that undergo the mixing.[66,67] One of these MOs needs to be occupied, and the other needs to be vacant, and they have to be fairly close in energy. The symmetry of the vibration leading from the pentagon to the trapezoidal structures is e_2'. By examining the MOs near the HOMO–LUMO gap in the anionic D_{5h} cluster (Fig. 5), we identified the HOMO (e_1') and the LUMO + 1 (e_2') in the spin-α set as the orbitals that we need. These MOs are *ca.* 1.0 eV apart in energy. Their direct product:

$$e_1' \otimes e_2'$$

produces a reducible representation that, upon acting with the projection operator, appears to contain the e_2' irreducible representation, corresponding to the vibration leading to the distorted planar structures. Furthermore, the LUMO + 1 is rich in the 6p-contributions, as seen from the expansions of the wave function as a linear combination of the atomic orbitals. Fig. 5 illustrates the onset of the second-order Jahn–Teller effect desymmetrizing the structure toward the trapezoid.

Thus, we establish that the formation of the distorted planar shape is facilitated by the engagement of the 6p-AOs on Pt into chemical bonding through the second-order Jahn–Teller effect. It is another way to say that the cluster exhibits partial covalency facilitated by 6sp-hybridization. The analogous exercise for the Zn-doped case is not possible, because the pentagonal and trapezoidal structures belong to the same symmetry point group in this case. However, we dare to generalize the effect to the Pt_4Zn^- cluster as well. Thus, even though the delocalized globular overlap is jeopardized in the planar structures, they are stabilized by the partial covalency instead, and this is the reason for the anions to go planar.

The fact that small metallic clusters can exhibit partial covalency is curious, and has been seen in a few cases so far.[60,61,68] The corresponding metals and alloys have metallic bonding and no signs of covalency in the bulk. When covalency is attainable, it is known to be a more stabilizing bonding effect than delocalized bonding, and so it makes cluster structures flat and distorted.[68]

However, from energy considerations, charging of clusters is not the only cause of their planarization upon surface deposition. Compare the energy differences between the lowest-energy 2-D and 3-D isomers of the anion in the gas phase (Fig. 3) to those of the formerly neutral (though charged by the support) clusters on the support (Fig. 1). The energy difference between the 3-D and 2-D isomers of the anionic gaseous clusters is 0.2 eV, comparing (b) and (c) in Fig. 3, and that of the

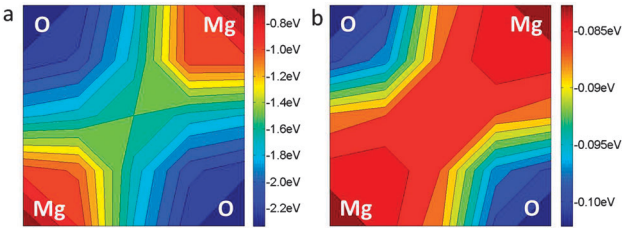

Fig. 6 PESs of (a) Pt and (b) Zn monomers on the MgO(100) surface. The unit cell contains two Mg and two O atoms, whose locations are labelled on the PESs. Note the difference in energy scales for the two monomers.

supported clusters is 0.65 eV, shown in Fig. 1, for Pt_5. For Pt_4Zn, it is 0.11 eV *versus* 0.5 eV, respectively. This indicates that the support provides constructive bonding interactions, further favouring planar structures.

One thing to observe from p-DOS (Fig. 4) is the development of covalent bonds between the Pt atoms and the O atoms in the MgO surface. These contributions to the p-DOS are outlined in red in Fig. 4. Maximizing these covalent interactions is key to the stabilization of planar structures provided by the support.

Finally, the reason why the sub-nanoclusters stand upright has to do with the matching of the cluster geometries with the positions of the surface oxygen atoms. Consider the potential energy surfaces (PESs) for the Pt and Zn monomers (uncharged) moving on the MgO(100) surface (Fig. 6). The regions of the O atoms are substantially more attractive than the regions near the Mg atoms for both monomers. Although it is a crude approximation to be thinking of individual monomers as models for atoms in the clusters, in clusters too, we see that the cluster–surface interactions happen at O atoms. Additionally, the wells on the PES for Pt are an order of magnitude deeper than those for Zn. This reflects the tendency of Pt to form covalent bonds to surface O atoms; O and Pt are closer in electronegativities than O and Zn are, and so when Pt and Zn atoms form a cluster, it is Pt that preferentially interacts with the support, despite the electrostatic attraction between the negatively charged O atoms and the positively charged Zn in the cluster. Next, putting the flat clusters down on the support would produce configurations where the Pt and Zn atoms from the top of the cluster would face contacts with surface Mg atoms. Therefore, horizontal structures are unfavourable, and clusters stand up-right. The configurations were artificially created where the clusters would lay flat; upon geometry optimizations these go to the up-right positions, indicating that there are not even metastable minima corresponding to horizontal clusters.

Conclusions

This theoretical study shows that Pt based clusters, Pt_5 and Pt_4Zn, change their shapes from the gas phase trigonal bi-pyramidal structure to planar trapezoidal that stand up on the MgO(100) surface. This phenomenon is uniquely observed in sub-nano Pt clusters on magnesia, and not seen for larger clusters. The morphology change is found to be due to several effects. First of all, it is cluster charging by taking *ca.* 1 *e* from the support, and anionic clusters in the gas phase are also flat. Planarization of the anions is due to recruitment of both 6s- and 6-p-AOs on Pt into chemical bonding leading to partial covalency, or a second order Jahn–Teller effect. Covalency is a strong bonding effect, due to its directional character; it is normally attributed to organic molecules, but recently has started to be recognized in all-metal clusters of very small sizes. This fundamental chemical bonding effect counteracts optimal delocalized bonding in defining cluster shapes, and, more specifically, drives clusters from globular to flat and distorted. In this work, we, for the first time, observe this effect in surface-deposited clusters. In view of the potential importance of the studied clusters in catalysis, covalency as a stabilizing and restructuring effect is important to recognize and desirable to use as a cluster design tool. Another contribution to the planarity of the deposited clusters is the maximization of the Pt–O covalent bonding with the surface. Due to matching of the positions of the cluster atoms and the lattice in the up-right structures, these configurations are preferred over the horizontal ones, where unfavourable interactions with the support would need to be accepted.

Acknowledgements

This work was supported by the AFOSR 10029173-S3 grant. ANA also thanks the Alfred P. Sloan Fellowship. Calculations were performed using the UCLA Hoffman2 shared cluster. A portion of research was performed using the EMSL, a national scientific user facility sponsored by the Department of Energy's Office of Biological and Environmental Research and located at Pacific Northwest National Laboratory.

Notes and references

1 G. Guisbiers, G. Abudukelimu and D. Hourlier, *Nanoscale Res. Lett.*, 2011, **6**, 396.
2 B. R. Cuenya, *Thin Solid Films*, 2010, **518**, 3127–3150.
3 (*a*) S. Yamazoe, K. Koyasu and T. Tsukuda, *Acc. Chem. Res.*, 2014, **47**, 816–824; (*b*) L. Xiao and L. C. Wang, *J. Phys. Chem. A*, 2004, **108**, 8605–8614.
4 W. E. Kaden, T. P. Wu, W. A. Kunkel and S. L. Anderson, *Science*, 2009, **326**, 826–829.
5 S. S. Lee, C. Y. Fan, T. P. Wu and S. L. Anderson, *J. Am. Chem. Soc.*, 2004, **126**, 5682–5683.
6 J. Zhang and A. N. Alexandrova, *J. Chem. Phys.*, 2011, **135**, 174702.
7 W. E. Kaden, W. A. Kunkel, M. D. Kane, F. S. Roberts and S. L. Anderson, *J. Am. Chem. Soc.*, 2010, **132**, 13097–13099.
8 L. Feng, D. T. Hoang, C. K. Tsung, W. Y. Huang, S. H. Y. Lo, J. B. Wood, H. T. Wang, J. Y. Tang and P. D. Yang, *Nano Res.*, 2011, **4**, 61–71.
9 O. S. Alexeev, G. W. Graham, M. Shelef and B. C. Gates, *J. Catal.*, 2000, **190**, 157–172.
10 B. R. Cuenya, S. H. Baeck, T. F. Jaramillo and E. W. McFarland, *J. Am. Chem. Soc.*, 2003, **125**, 12928–12934.

11 A. Kulkarni, R. J. Lobo-Lapidus and B. C. Gates, *Chem. Commun.*, 2010, **46**, 5997–6015.
12 J. Zhang and A. N. Alexandrova, *J. Phys. Chem. Lett.*, 2013, **4**, 2250–2255.
13 J. Zhang and A. N. Alexandrova, *J. Phys. Chem. Lett.*, 2012, **3**, 751–754.
14 F. A. Cotton and T. E. Haas, *Inorg. Chem.*, 1964, **3**, 10.
15 M. C. Dossantos and J. A. O. Deaguiar, *Z. Phys. D: At., Mol. Clusters*, 1989, **12**, 391–394.
16 Y. G. Wang, Y. Yoon, V. A. Glezakou, J. Li and R. Rousseau, *J. Am. Chem. Soc.*, 2013, **135**, 10673–10683.
17 B. Yoon, H. Hakkinen, U. Landman, A. S. Worz, J. M. Antonietti, S. Abbet, K. Judai and U. Heiz, *Science*, 2005, **307**, 403–407.
18 M. M. Bhasin, J. H. McCain, B. V. Vora, T. Imai and P. R. Pujado, *Appl. Catal., A*, 2001, **221**, 397–419.
19 V. Galvita, G. Siddiqi, P. P. Sun and A. T. Bell, *J. Catal.*, 2010, **271**, 209–219.
20 R. Burch and L. C. Garla, *J. Catal.*, 1981, **71**, 360–372.
21 O. A. Barias, A. Holmen and E. A. Blekkan, *J. Catal.*, 1996, **158**, 1–12.
22 E. L. Jablonski, A. A. Castro, O. A. Scelza and S. R. de Miguel, *Appl. Catal., A*, 1999, **183**, 189–198.
23 P. P. Sun, G. Siddiqi, W. C. Vining, M. F. Chi and A. T. Bell, *J. Catal.*, 2011, **282**, 165–174.
24 G. Siddiqi, P. P. Sun, V. Galvita and A. T. Bell, *J. Catal.*, 2010, **274**, 200–206.
25 H. Ren, M. P. Humbert, C. A. Menning, J. G. Chen, Y. Y. Shu, U. G. Singh and W. C. Cheng, *Appl. Catal., A*, 2010, **375**, 303–309.
26 M. R. Jovanovic and P. S. Putanov, *Appl. Catal., A*, 1997, **159**, 1–7.
27 P. L. De Cola, R. Glaser and J. Weitkamp, *Appl. Catal., A*, 2006, **310**, 205–206.
28 J. F. Goellner, K. M. Neyman, M. Mayer, F. Nortemann, B. C. Gates and N. Rosch, *Langmuir*, 2000, **16**, 2736–2743.
29 C. T. Campbell, *Acc. Chem. Res.*, 2013, **46**, 1712–1719.
30 J. Goniakowski and C. Mottet, *J. Cryst. Growth*, 2005, **275**, 29–38.
31 W. Vervisch, C. Mottet and J. Goniakowski, *Eur. Phys. J. D*, 2003, **24**, 311–314.
32 C. Gatel, P. Baules and E. Snoeck, *J. Cryst. Growth*, 2003, **252**, 424–432.
33 P. Giannozzi, S. Baroni, N. Bonini, M. Calandra, R. Car, C. Cavazzoni, D. Ceresoli, G. L. Chiarotti, M. Cococcioni, I. Dabo, A. Dal Corso, S. de Gironcoli, S. Fabris, G. Fratesi, R. Gebauer, U. Gerstmann, C. Gougoussis, A. Kokalj, M. Lazzeri, L. Martin-Samos, N. Marzari, F. Mauri, R. Mazzarello, S. Paolini, A. Pasquarello, L. Paulatto, C. Sbraccia, S. Scandolo, G. Sclauzero, A. P. Seitsonen, A. Smogunov, P. Umari and R. M. Wentzcovitch, *J. Phys.: Condens. Matter*, 2009, **21**, 395502.
34 W. Kohn and L. J. Sham, *Phys. Rev.*, 1965, **140**, 1133.
35 C. T. Lee, W. T. Yang and R. G. Parr, *Phys. Rev. B: Condens. Matter Mater. Phys.*, 1988, **37**, 785–789.
36 K. Burke, J. Werschnik and E. K. U. Gross, *J. Chem. Phys.*, 2005, **123**, 062206.
37 J. P. Perdew, K. Burke and M. Ernzerhof, *Phys. Rev. Lett.*, 1996, **77**, 3865–3868.
38 W. Tang, E. Sanville and G. Henkelman, *J. Phys.: Condens. Matter*, 2009, **21**, 084204.
39 E. Sanville, S. D. Kenny, R. Smith and G. Henkelman, *J. Comput. Chem.*, 2007, **28**, 899–908.
40 G. Henkelman, A. Arnaldsson and H. Jonsson, *Comput. Mater. Sci.*, 2006, **36**, 354–360.
41 J. M. Tao, J. P. Perdew, V. N. Staroverov and G. E. Scuseria, *Phys. Rev. Lett.*, 2003, **91**, 146401.
42 D. Hegarty and M. A. Robb, *Mol. Phys.*, 1979, **38**, 1795–1812.
43 R. H. A. Eade and M. A. Robb, *Chem. Phys. Lett.*, 1981, **83**, 362–368.
44 H. B. Schlegel and M. A. Robb, *Chem. Phys. Lett.*, 1982, **93**, 43–46.
45 F. Bernardi, A. Bottoni, J. J. W. Mcdouall, M. A. Robb and H. B. Schlegel, *Faraday Symp. Chem. Soc.*, 1984, **19**, 137–147.
46 M. Frisch, I. N. Ragazos, M. A. Robb and H. B. Schlegel, *Chem. Phys. Lett.*, 1992, **189**, 524–528.
47 N. Yamamoto, T. Vreven, M. A. Robb, M. J. Frisch and H. B. Schlegel, *Chem. Phys. Lett.*, 1996, **250**, 373–378.
48 C. Moller and M. S. Plesset, *Phys. Rev.*, 1934, **46**, 0618–0622.
49 M. Headgordon, J. A. Pople and M. J. Frisch, *Chem. Phys. Lett.*, 1988, **153**, 503–506.
50 S. Saebo and J. Almlof, *Chem. Phys. Lett.*, 1989, **154**, 83–89.
51 M. J. Frisch, M. Headgordon and J. A. Pople, *Chem. Phys. Lett.*, 1990, **166**, 275–280.
52 M. J. Frisch, M. Headgordon and J. A. Pople, *Chem. Phys. Lett.*, 1990, **166**, 281–289.
53 M. Head-Gordon and T. Head-Gordon, *Chem. Phys. Lett.*, 1994, **220**, 122–128.
54 K. A. Peterson and C. Puzzarini, *Theor. Chem. Acc.*, 2005, **114**, 283; D. Figgen, G. Rauhut, M. Dolg and H. Stoll, *Chem. Phys.*, 2005, **311**, 227.
55 M. J. Frisch, G. W. Trucks, H. B. Schlegel, G. E. Scuseria, M. A. Robb, J. R. Cheeseman, G. Scalmani, V. Barone, B. Mennucci, G. A. Petersson, H. Nakatsuji, M. Caricato, X. Li, H. P. Hratchian, A. F. Izmaylov, J. Bloino, G. Zheng, J. L. Sonnenberg, M. Hada, M. Ehara, K. Toyota, R. Fukuda, J. Hasegawa, M. Ishida, T. Nakajima, Y. Honda, O. Kitao, H. Nakai, T. Vreven, J. A. Montgomery, Jr., J. E. Peralta, F. Ogliaro, M. Bearpark, J. J. Heyd, E. Brothers, K. N. Kudin, V. N. Staroverov, R. Kobayashi, J. Normand, K. Raghavachari, A. Rendell, J. C. Burant, S. S. Iyengar, J. Tomasi, M. Cossi, N. Rega, J. M. Millam, M. Klene, J. E. Knox, J. B. Cross, V. Bakken, C. Adamo, J. Jaramillo, R. Gomperts, R. E. Stratmann, O. Yazyev, A. J. Austin, R. Cammi, C. Pomelli, J. W. Ochterski, R. L. Martin, K. Morokuma, V. G. Zakrzewski, G. A. Voth, P. Salvador, J. J. Dannenberg, S. Dapprich, A. D. Daniels, Ö. Farkas, J. B. Foresman, J. V. Ortiz, J. Cioslowski and D. J. Fox, *Gaussian 09, Revision D.01*, Gaussian, Inc., Wallingford, CT, 2009.
56 A. N. Alexandrova, *J. Phys. Chem. A*, 2010, **114**, 12591–12599.
57 I. B. Bersuker, *Chem. Rev.*, 2001, **101**, 1067.
58 I. B. Bersuker, *The Jahn–Teller Effect*, Cambridge University Press, Cambridge, U.K., 2006.

59 J. E. Boggs and V. Z. Polinger, *The Jahn–Teller Effect and Beyond: Selected Works of Isaac Bersuker with Commentaries*, The Academy of Sciences of Moldova, Chisnau, Moldova, 2008.
60 A. N. Alexandrova and A. I. Boldyrev, *J. Chem. Theory Comput.*, 2005, **1**, 566–580.
61 A. N. Alexandrova, A. I. Boldyrev, X. A. Li, H. W. Sarkas, J. H. Hendricks, S. T. Arnold and K. H. Bowen, *J. Chem. Phys.*, 2011, **134**, 044322.
62 S. N. Khanna and P. Jena, *Phys. Rev. Lett.*, 1992, **69**, 1664–1667.
63 A. N. Alexandrova, *Chem. Phys. Lett.*, 2012, **533**, 1–5.
64 A. N. Alexandrova, M. J. Nayhouse, M. T. Huynh, J. L. Kuo, A. V. Melkonian, G. Chavez, N. M. Hernando, M. D. Kowal and C. P. Liu, *Phys. Chem. Chem. Phys.*, 2012, **14**, 14815–14821.
65 E. D. Glendening, A. E. Reed, J. E. Carpenter and F. Weinhold, NBO Version 3.1.
66 A. S. Ivanov, K. V. Bozhenko and A. I. Boldyrev, *Inorg. Chem.*, 2012, **51**, 8868–8872.
67 A. P. Sergeeva and A. I. Boldyrev, *Organometallics*, 2010, **29**, 3951–3954.
68 M. T. Huynh and A. N. Alexandrova, *J. Phys. Chem. Lett.*, 2011, **2**, 2046–2051.

